ACTIVE 97
BUDAPEST–HUNGARY
1997 AUGUST 21–23

OPTIMAL LOCATION OF PZT ACTUATOR FOR THE PVDF BASED WAVENUMBER SENSING APPROACH IN ACTIVE SOUND RADIATION CONTROL

Bor-Tsuen Wang

Department of Mechanical Engineering
National Pingtung Polytechnic Institute
Pingtung, Taiwan 91207
Republic of China

ABSTRACT

This paper determines the optimal location of PZT actuators in conjunction with the use of PVDF based wavenumber sensing approach for active sound radiation control of a simply-supported beam. The PVDF based wavenumber sensing is first briefly reviewed. The optimization problem for the optimum positioning of the PZT actuator is then formulated. The genetic algorithm (GA), a general optimization procedure is adopted to determine the optimal location of PZT actuators incorporated with linear quadratic optimal control theory (LQOCT) to obtain the optimal control voltage, when the location of the PZT actuator is determined. The optimal location of PZT actuators are successfully determined in considering four types of cost functions associated with the wavenumber sensing approaches. The control performance of the optimally positioned PZT actuators is compared with that of the arbitrarily selected ones. Results show that the optimally located PZT actuators can greatly reduce the radiated power. In particular, for the off-resonance excitation cases the reduction of radiated power can be up to 10 dB. The control mechanisms of the optimum PZT actuators are also studied by examining the sound pressure level (SPL) distributions and the wavenumber transform spectra. This work enhances the sensing and actuation abilities and leads to the optimum design of intelligent material structure systems for active structural acoustic control.
keywords: piezoceramic transducers, optimum design, wavenumber, active structural acoustic control, intelligent material structure system

INTRODUCTION

The development of intelligent materials structure systems (IMSS) is of great interest [1,2]. The actuators and sensors can be imbedded or attached to the structures, so as to perform active control of structural vibration and sound radiation. The PZT actuator and PVDF sensor are one of the frequently used materials for the IMSS. The IMSS for active structural acoustic control (ASAC) has also been of concern. The design of various types of control

actuators and sensors are developed for different purposes of applications. The PZT actuator and PVDF sensor are increasingly applied as the control transducers for ASAC and have been shown many advantages over the conventional transducers, such as point force and microphones [3,4].

Because of the strong correlation between structural vibration and sound radiation, various types of structural sensors have been developed and used for structural sound radiation control [5-8]. The accelerometers are conventionally used and adhered to the structure surface to measure the point acceleration that is composed as the error signal for active control applications [9,10]. However, the cost, mass inertia effect and practical implementation for the accelerometer are its deficiencies. The PVDF film sensors that are thin, light weight and low cost can be adhered to the structure surface to measure the structure response. A strip type [8,11,12] or shaped PVDF sensor [8,13] was developed and shown much potential in active vibration and acoustic controls.

The wavenumber domain sensing approach has been shown a promising way of obtaining the efficient error signal for ASAC. As known, the supersonic wavenumber component that will contribute to the sound radiation into the far-field. In contrast, the subsonic wavenumber components will not radiate into the far field [14]. The wavenumber domain control was first proposed by Fuller and Burdisso [15]. With the use of a microphone as the error sensor, a cost function is defined as the wavenumber component corresponding to the radiation angle of the microphone. The minimization of the wavenumber component is similar to the minimization of the radiated sound pressure at the prescribed angle. Fuller and Maillard [16,17] applied a series of accelerometers and performed discrete wavenumber transform on the acceleration signals to obtain the wavenumber components. Those wavenumber components can then be adopted to construct the cost function that is to be minimized for structural sound radiation control. Wang [18] developed an PVDF based wavenumber sensing approach for active sound radiation control of a simply-supported beam. A series of PVDF strip sensors are equally spaced and distributed over the beam length. By performing the discrete wavenumber transform on the PVDF sensor signals, the PVDF wavenumber transform function can be obtained. The sum of mean square value of PVDF wavenumber transform function in the supersonic region is then defined as the cost function. Wang [18] showed that the PVDF based wavenumber sensing technique is efficient for sound radiation control of a simply supported beam. Wang [18] also indicated that for some off-resonance excitation cases the control can be inefficient due to the improper location PZT actuator. For the application of PVDF strip sensors to the wavenumber sensing approach, the length and thickness of PVDF sensors have been shown little effect on the control performance. Therefore, the optimal location of PZT actuator become of interest to improve the control performance, in particular for the off-resonance excitation.

This work first formulates the optimization problem for the optimum positioning of the PZT actuator. The length of PZT actuator is assumed to be fixed, and so forth the central location of the PZT actuator is selected as the design variable. The genetic algorithm (GA) is then applied to solve for the optimal location of PZT actuator in conjunction with the linear quadratic optimal control theory (LQOCT) to determine the control voltage input to the PZT actuator. The control efficiency is shown greatly improved. The actuation and sensing abilities of the IMSS can then be greatly enhanced.

WAVENUMBER DOMAIN SENSING APPROACH

By performing continuous wavenumber transform (CWT) in terms of spatial coordinates for a two-dimensional rectangular radiator, the acceleration wavenumber transform function, $\tilde{A}$, can be obtained as follows by neglecting the harmonic time function:

$$\tilde{A}(\kappa_x,\kappa_y)=\int_{-\infty}^{\infty}\int_{-\infty}^{\infty}\ddot{w}(x,y)e^{-i(\kappa_x x+\kappa_y y)}dxdy \tag{1}$$

where

$$\kappa_x=\kappa\sin\theta\cos\phi \tag{2}$$

$$\kappa_y=\kappa\sin\theta\sin\phi \tag{3}$$

and $\ddot{w}$ represents the acceleration of the radiator. For a one-dimensional beam application as shown in Figure 1, the y-direction response is negligible; therefore, the beam acceleration wavenumber transform function (WTF), by performing the continuous wavenumber transform and neglecting the time component, can be expressed as [18]:

$$\tilde{A}(\kappa_x,\kappa_y)=-\omega^2\left[\frac{e^{-j\kappa_y b}-1}{-j\kappa_y}\right]\sum_{n=1}^{\infty}q_n(\omega)\tilde{\phi}_n(\kappa_x) \tag{4}$$

where

$$\tilde{\phi}_n(\kappa_x)=\int_{-\infty}^{\infty}\phi_n(x)e^{-j\kappa_x x}dx=\int_0^L\phi_n(x)e^{-j\kappa_x x}dx=\alpha_n\left[\frac{1-(-1)^n e^{-i\kappa_x L}}{\alpha_n^2-\kappa_x^2}\right] \tag{5}$$

in which $\alpha_n=n\pi/L$, and $q_n(\omega)$ is modal amplitude depending on the external force. $\tilde{\phi}_n(\kappa_x)$ is the continuous wavenumber transform of the mode shape function of the simply-supported beam, $\phi_n(x)$, and can be approximated by the discrete wavenumber transform (DWT) as follows:

$$\tilde{\phi}_n(m\Delta\kappa_x)=\sum_{i=1}^{N}\phi_n(i\Delta x)e^{-j\left(\frac{mi}{N}\right)}\Delta x\ , \qquad m=-(N-1),-(N-2),\ldots,-1,0,1,\ldots,N-1 \tag{6}$$

where

$$\Delta\kappa_x=\frac{1}{L} \tag{7}$$

$$N=\frac{L}{\Delta x} \tag{8}$$

N is the number of discretization, i.e., the number of sensors applied in practical measurement; and Δx is the equal distance between accelerometers. The acceleration WTF by performing the DWT for κ_y-0 can then be derived:

$$\tilde{A}_{DWT}(m\Delta\kappa_x)-jb\omega^2\sum_{n-1}^{\infty} q_n(\omega)\tilde{\phi}_n(m\Delta\kappa_x) \qquad m=-(N-1),-(N-2),\ldots,-1,0,1,\ldots,N-2,N-1 \quad (9)$$

It is noted that the negative wavenumber components (m = negative integer) are also included and simply correspond to radiation in opposite directions than the positive wavenumber ones.

Similarly, the generated voltages from the PVDF film [18] can also be taken by the CWT in κ-plane and derived as follows:

$$\tilde{V}(\kappa_x,\kappa_y)-K_p[\frac{e^{-j\kappa_y b}-1}{-j\kappa_y}]\sum_{n-1}^{\infty} q_n(\omega)\tilde{\phi}_n^p(\kappa_x) \quad (10)$$

where

$$\tilde{\phi}_n^p(\kappa_x)-\int_0^L \phi_n^p(x)e^{-j\kappa_x x}dx-2\alpha_n^2\sin(\alpha_n l_p/2)[\frac{1-(-1)^n e^{-i\kappa_x L}}{\alpha_n^2-\kappa_x^2}] \quad (11)$$

in which $\phi_n^p(x)$ is the PVDF mode shape function; K_p is some constant related to the physical properties of PVDF sensor [19]. Again, the continuous wavenumber transform of the PVDF voltage shown in Equation (10) can be approximated by the discrete wavenumber transform; therefore, the PVDF voltage WTF by performing the DWT for κ_y-0 can be obtained

$$\tilde{V}_{DWT}(m\Delta\kappa_x)=-jb\sum_{n-1}^{\infty} q_n(\omega)\tilde{\phi}_n^p(m\Delta\kappa_x)\ , \qquad m=-(N-1),-(N-2),\ldots,-1,0,1,\ldots,N-2,N-1 \quad (12)$$

where

$$\tilde{\phi}_n^p(m\Delta\kappa_x)-\sum_{i-1}^{N}\phi_n^p(i\Delta x)e^{-j(\frac{mi}{N})}\Delta x\ , \qquad m=-(N-1),-(N-2),\ldots,-1,0,1,\ldots,N-2,N-1 \quad (13)$$

$\tilde{\phi}_n^p(m\Delta\kappa_x)$ denotes the m-th wavenumber components of the PVDF mode shape $\phi_n^p(x)$ by performing the discrete wavenumber transform; and $i\Delta x$ is the spatial coordinate of the i-th sensor location.

COST FUNCTIONS

It is noted that the mean square value of the acceleration wavenumber transform function, i.e., $|\tilde{A}|^2$, integrated over the supersonic region is related to the radiated power [14]. Only the wavenumber components satisfying $\kappa_x^2+\kappa_y^2<\kappa^2$ contribute to sound radiation into the far-field, and are termed as the supersonic waves. The other wavenumber components associated with subsonic waves do not radiate into the far-field. For a one-dimensional beam with infinite rigid baffle, the radiated power can be expressed in terms of the wavenumber transform of beam acceleration as follows [20]:

$$\Phi_p = \frac{\rho c \kappa}{4\pi\omega^2}\int_{-\kappa}^{\kappa}\frac{|\tilde{A}(\kappa_x)|^2}{\sqrt{\kappa^2-\kappa_x^2}}d\kappa_x \tag{14}$$

It is difficult to exactly evaluate the above integral. Cremer and Heckl [20] provided an approximate method to estimate the radiated power. Here, it is reasonable to construct the cost function based on the wavenumber transform functions introduced in Equations (4) and (10). Two types of cost functions associated with the wavenumber components in supersonic region are defined as follows:

$$\Phi_{\kappa,\tilde{A}} = \int_{-\kappa}^{\kappa}|\tilde{A}(\kappa_x,\kappa_y=0)|^p d\kappa_x \tag{15}$$

$$\Phi_{\kappa,\tilde{V}} = \int_{-\kappa}^{\kappa}|\tilde{V}(\kappa_x,\kappa_y=0)|^p d\kappa_x \tag{16}$$

It is noted that $\Phi_{\kappa,\tilde{A}}$ is the integration of supersonic wavenumber components that contribute to the sound radiation into the far-field, and is strongly related to the radiated power. $\Phi_{\kappa,\tilde{V}}$ is the integration of the mean square value of PVDF voltage wavenumber transform functions over the supersonic region. By examining Equations (4) and (10), there are two main differences. Firstly, constants $-\omega^2$ and K_p are pre-multiplied for $\tilde{A}$ and $\tilde{V}$ respectively. Secondly, $\tilde{\phi}_n(\kappa_x)$ and $\tilde{\phi}_n^p(\kappa_x)$ are for $\tilde{A}$ and $\tilde{V}$ in the summation respectively. $\tilde{\phi}_n(\kappa_x)$ and $\tilde{\phi}_n^p(\kappa_x)$ are obtained by performing the wavenumber transform on $\phi_n(x)$ and $\phi_n^p(x)$. It is noted that $\phi_n^p(x)$ is the slope difference between the two edges of the PVDF film. In particular, $\phi_n^p(x)$ is related to the displacement mode shape $\phi_n(x)$ for the case of simply-supported beam. From the comparison between Equations (5) and (11), one can see that $\tilde{\phi}_n(\kappa_x)$ and $\tilde{\phi}_n^p(\kappa_x)$ have the same form of functions in terms of κ_x; therefore, cost functions $\Phi_{\tilde{A}}$ and $\Phi_{\tilde{V}}$ can be strongly correlated and also related to the radiated power, as shown in Equation (14). Both $\Phi_{\kappa,\tilde{A}}$ and $\Phi_{\kappa,\tilde{V}}$ are continuous functions obtained from the acceleration and PVDF voltage wavenumber transform functions, based on the CWT approach. It is noted that these two cost functions can not be measured directly in reality, although these cost functions are highly correlated to the structural sound radiation.

With the use of a series of evenly spaced accelerometers or PVDF strip film sensors in conjunction with the DWT approach, the discrete wavenumber transform functions based on accelerometers and PVDF sensors can be derived through Equations (4) and (10), and shown in Equations (9) and (12). Both negative and positive wavenumber components can be obtained. In fact, because of the symmetry of wavenumber spectrum and folding effect of discrete wavenumber transform (analogy to the time domain Fourier transform), the negative wavenumber components can also be obtained without the operation of discrete wavenumber transform on the negative integer m. Notice that only the wavenumber components below and above the Nyquist wavenumber $\pm\kappa_{x,Nyq} = \frac{N}{2}\Delta\kappa_x$ are valid. Analogy to Equations (15) and (16) for the CWT approach, the cost functions based on the DWT approach for accelerometers and PVDF sensors can be defined as

$$\Phi_{\kappa,\tilde{A}_{DWT}} = \sum_{m=-N_k}^{N_k} |\tilde{A}_{DWT}(m\Delta\kappa_x)|^2 , \qquad \min(N_k) > \frac{\kappa}{\Delta\kappa_x} + 1 \tag{17}$$

$$\Phi_{\kappa,\tilde{V}_{DWT}} = \sum_{m=-N_k}^{N_k} |\tilde{V}_{DWT}(m\Delta\kappa_x)|^2 , \qquad \min(N_k) > \frac{\kappa}{\Delta\kappa_x} + 1 \tag{18}$$

$\Phi_{\kappa,\tilde{A}_{DWT}}$ and $\Phi_{\kappa,\tilde{V}_{DWT}}$ represent the sum of mean square values of the supersonic wavenumber components of the acceleration and PVDF voltage WTFs respectively; and N_κ is the minimum number of wavenumber components, such that $\min(N_k) > \frac{\kappa}{\Delta\kappa_x} + 1$. It is noted that $\Phi_{\kappa,\tilde{A}_{DWT}}$ and $\Phi_{\kappa,\tilde{V}_{DWT}}$ are measurable, and can be used to approximate the cost functions $\Phi_{\kappa,\tilde{A}}$ and $\Phi_{\kappa,\tilde{V}}$. In Summary, $\Phi_{\kappa,\tilde{A}}$ and $\Phi_{\kappa,\tilde{V}}$ derived from the CWT approach are ideal cost functions, which are not measurable. $\Phi_{\kappa,\tilde{A}_{DWT}}$ and $\Phi_{\kappa,\tilde{V}_{DWT}}$ are defined from the acceleration and PVDF voltage WTFs by the DWT approach, and can be obtained by using a series of equally spaced accelerometers and PVDF sensors respectively.

Any one of the cost functions mentioned above is obviously quadratic and positively definite and possesses a unique minimum. The linear quadratic optimal control theory (LQOCT) can then be applied to minimize the cost function, so as to find the optimal control voltages input to the piezoelectric actuators. One can easily perform minimization procedures [21] to calculate the optimal control parameters, so as to minimize the cost function. The full analysis can be referred to [22] and is omitted here for brevity.

FORMULATION OF OPTIMIZATION PROBLEM

Genetic Algorithm. The genetic algorithm is derived based on Darwin's theory of "Survival of the Fittest" [23]. The GA is a search procedure for general optimization problems and is numerically simple involving nothing more than random number generation, bit manipulation and string exchange. The objective function is usually transformed to a fitness function

$$F(x) = base\ value - f(x) \tag{19}$$

The GA is to maximize the fitness function, $F(x)$, in contrast to minimize the objective function, $f(x)$, in comparison with the traditional optimization procedures. The design variables, x, are encoded as a binary digit string which is analogous to chromosome in a biological system. When multiple design variables are desired, all design variables are concatenated to one single string. In the beginning, the GA randomly generates a population of strings by successive coin flips. The generation process is then succeeded to produce the new generation of population by performing three basic operators of GA: reproduction, crossover, and mutation. Strings can be decoded to obtain the exact values of the design variables in order to calculate the fitness values. The design constraints can be treated by the exterior penalty function method such that a constrained problem is transformed to an unconstrained problem.

Optimization Problem for Optimal Location of PZT Actuator. As shown in Figure 1, a simply-supported beam in an infinite rigid baffle is considered as the plant subjected to a harmonically excited point force disturbance. The sound radiation from the beam is controlled by PZT actuators in conjunction with the use of LMS feedforward control algorithm, while the accelerometer and PVDF based wavenumber sensing approaches are adopted. The size of the i-th PZT actuator is assumed to be fixed. The applied voltages to the piezoelectric actuators can be calculated from linear quadratic optimal control theory (LQOCT). Therefore, the design variables can be identified as:

$$\bar{x}_1, \bar{x}_2, \ldots, \bar{x}_{N_c} \tag{20}$$

where $\bar{x}_i$ are the central location of the i-th PZT actuator. The objective function can then be defined as the total radiated sound power as shown in Equation (33) and transformed to a fitness function as shown in Equation (19). The bounds of design variables can be inherently implemented, and the unconstrained optimization problem can be completely defined. Therefore, the genetic algorithm can then be applied to determine the optimal locations of PZT actuators and microphone sensors. The solution strategy is described as follows.

Implementation of Genetic Algorithm. The GA is implemented as FORTRAN codes incorporated with the use of LQOCT for the calculation of the optimal control voltages input to actuators whenever the locations of actuators are determined. The solution flow chart is shown in Figure 2 [24]. The detail procedure is described as follows:

1. Setup GA constants. At the beginning of the program, some GA constants including population size for each generation, the string length of design variables, crossover probability, mutation probability and the number of maximum generation must be specified.
2. Generate initial population. The binary digit string is generated by successive coin flips. The design variables are encoded as a binary digit string. All design variables are concatenated to one single string.
3. Calculate the population statistics. In this stage, each string is decoded to obtain the exact values of design variables, which are the central locations of PZT actuators and the radial angles of microphone sensors. The LQOCT is then applied to calculate the control voltages input to the PZT actuators for each one string contained in the populations. The fitness function for each string can also be computed. Finally, the maximum, averaged, minimum and sum of the fitness for the current generation can be obtained. Those values are required in the production of new generation.
4. Produce new generation. To produce a new generation, three basic GA operators, i.e., reproduction, crossover and mutation, are performed. A pair of reproduction mates are first selected by a roulette wheel with slots sized according to the fitness values. The crossover is then performed for the selected reproduction mates based on the crossover probability. Finally, the mutation is performed on the children sets to produce the new generation array.
5. Calculate the population statistics. The procedures are the same as those in Step 3.
6. Report results. This stage is to print out the results of population statistics as well as the string digit and the exact values of design variables for further analysis.
7. Repeat Steps 4 to 6 until the program reaches the number of maximum generation.

RESULTS AND DISCUSSIONS

A steel beam with length of 0.38m, width of 0.04m, and thickness of 2mm is used in the simulations. The first few natural frequencies are 33.2 Hz, 128.8 Hz, 289.9 Hz, 515.4 Hz, 805.3 Hz and 1159.6 Hz. It is noted that no damping was included in the following analysis. A harmonic point force with input parameters, $F=0.3$N and $x_f=0.067$m, was considered as the disturbance input for the following analysis. The piezoceramic patch (G-1195) [25] and PVDF films (LDT-28 μk) [26] are used respectively. The piezoceramic patch is located at $x_1=0.285$m, $x_2=0.3485$m for the arbitrarily selected case. In order to achieve the wavenumber sensing approach, a series of PVDF strip films are evenly distributed over the beam length as shown in Figure 1. The PVDF strip film is assumed to be 0.02m in length for wavenumber sensing approaches. For the purpose of comparison, a series of accelerometers are also used and assumed to be located at the central location of PVDF films, so as to perform the wavenumber sensing approach. Both the radiation directivity and WTF distributions are shown to demonstrate the control mechanisms of the wavenumber sensing approaches. The radiated sound pressure is calculated at a radial distance of 3m from the beam, and plotted in dB *re* 20×10^{-6} Pa over $\theta=-90^\circ$ to 90° for $\phi=0^\circ$.

The optimal location of PZT actuators for the four types of cost functions are shown in Figure 3, and their values are listed in Tables 1 and 2. The PZT actuators are depicted in Figure 3, the associated structural mode shape are also shown. For the cost function of Φ_A, several remarks can be made as follows:

1. For on-resonance excitation cases, i.e., 33.2 Hz, 128.8 Hz and 290 Hz corresponding to the first, second and third resonance modes, one edge of the PZT actuator is near to the maximum response of the associated structural mode shape. This agrees with the conclusions of previous works [27-29].
2. For off-resonance excitation cases, the PZT actuator is located right between the locations associated to the on-resonance excitation cases. This can be postulated that the optimal location of the PZT actuator is determined under a comprise to eliminate the significant response of structural modes. The control mechanisms will be further discussed later.
3. As the excitation frequency increases, the optimal location of PZT actuator is shifted to the left gradually. As known, the lower structural modes usually have higher radiation efficiency [30-32]. Therefore, the optimal location of PZT actuator is determined to minimize the significant modal response and to be shifted to the left.

For the case of $\Phi_{\tilde{p}}$, the cost function is obtained by the CWT approach similar to Φ_A, but the PVDF ideal sensors are assumed instead of ideal acceleration sensors. Previous work [18] shows that the cost function $\Phi_{\tilde{p}}$ related to the radiated power is a proper candidate as the cost function to perform active sound radiation control. The optimal location of PZT actuator for the case of $\Phi_{\tilde{p}}$ for different excitation frequencies are depicted as shown on the second column of Figure 3. One can see that the optimal locations of PZT actuators are quite similar to those for the case of Φ_A. This can be explained that the nature of the two cost functions are physically similar, because they have the same form of functions in terms

of structural wavenumbers [18]. An interesting result is that the optimal location of the PZT actuator is near the end of the boundary of the beam for the third resonance excitation case. This is not much surprising for such a location that is still an optimum candidate according to the previous works [27-29].

For the DWT approach associated with the accelerometer and PVDF based wavenumber domain sensing, the number of sensor is assumed to be 10 as depicted and shown in Figure 3. The optimal location of PZT actuators can also be found by the previous method discussed. There is only slight difference from the CWT approach and can be concluded that the DWT approach is well enough to approximate the CWT approach. The wavenumber domain sensing can therefore be practically carried out by the evenly distributed accelerometers or PVDF sensors.

To further examine the performance of optimized PZT actuator, the reduction of the radiated power for the four cases as shown in Table 3 is compared with the arbitrarily selected ones that is based on the cost function of $\Phi_{\tilde{A}}$. Some observations are made as follows:

1. The CWT approach can provide better sound radiation control than the DWT approach for the optimal positioning of the PZT actuators.
2. The accelerometer based wavenumber sensing generally achieved more reduction of the radiated power than the PVDF ones, because the acceleration wavenumber transform function is more related to the form of the radiated power than the PVDF ones.
3. $\Phi_{\tilde{A}}$ can provide the most reduction of radiated power than other types of cost functions for its strong links to the radiated power.
4. $\Phi_{\tilde{A}}$ is the best choice as the cost functions among the four types of cost functions, though it is not practically applicable. The arbitrarily selected sets of PZT actuators for control application is chosen to compare with and to evaluate the optimally positioned PZT actuators.
5. A large amount of radiated power can be reduced for on-resonance excitation for the arbitrarily selected actuators; however, only a small amount or almost none of reduction of radiated power can be obtained for off-resonance excitation cases. This has been indicated by the author in the previous work [18]. One can see that for the optimized cases either on- or off-resonance excitation can achieve much more reduction of radiated power than the arbitrarily ones.

The optimal location of PZT actuator is determined and their effect on the reduction of radiated power is discussed. The effect of the location of PZT actuator on the control performance can be further studied by examining the SPL distributions and acceleration wavenumber transform spectra. Figure 4 shows the SPL distributions for different excitation frequencies considering the optimum design of PZT actuators for the four types of cost functions and the arbitrarily selected ones. Figure 4(a) is for the first resonance excitation case. As mentioned, the central location of the arbitrary PZT actuator is located at one sixth of the beam, i.e., the maximum response of the third structural mode shape. The PZT actuator at such a location can well attenuate the significant radiation modes, i.e., the first mode here. For the CWT and DWT approaches with the use of the optimum PZT actuators, the dip near $\theta=0^{\circ}$ can be clearly observed. The dips indicate that the second radiation mode

is actually amplified, while the first mode is well controlled. Figure 5(a) also shows the acceleration wavenumber transform spectra corresponding to the case of Figure 4(a). The dips at κ_r-0 after being controlled, which corresponds to the radiation angle θ-0°, thus explains the SPL distributions. It is also noted that the wavenumber components in the supersonic region, i.e., $-\kappa<\kappa_r<\kappa$, are greatly reduced, and thus a large amount of reduction of radiated power can be obtained.

For other frequencies excitation cases, the similar observation and discussions can be made. It is worth to further discuss the off-resonance excitation cases, because the optimization is mainly for the need of control inefficiency of off-resonance excitation. For the case of f=230Hz, i.e., between the second and third structural resonances, the disturbance reveals a monopole response but a small dip near θ-0° that evidences the existence of the second mode. The arbitrarily selected PZT actuators will not achieve efficient control, and only 0.01 dB reduction of the radiated power can be seen from Table 3. From Table 3, one can also observe that over 10 dB reduction of radiated power can be obtained for the off-resonance excitation cases. The global reduction of SPL distributions can be also seen about 10 dB from Figure 4(d). As discussed previously, the optimal location of PZT actuator is determined under a compromise to attenuate the second and third modes simultaneously. As observed from Figure 4(d), the residual SPL reveals the third mode response and, therefore, indicates the second mode is well controlled leaving the third mode as the significant ones.

CONCLUSIONS

This work applies the genetic algorithm in conjunction with the LQOCT to optimally determine the optimum position of PZT actuators for the accelerometer and PVDF based wavenumber domain sensing approaches in active structural acoustic control. Four types of cost functions associated with wavenumber domain sensing for both the CWT and DWT approaches are considered. The optimal positioning of the PZT actuator can greatly improve the control efficiency. In particular, for off-resonance excitation the radiated power can be obtained over 10 dB after the PZT actuator being optimized. The control mechanisms of the optimum PZT actuator are studied and characterized through the analysis of the SPL distributions and acceleration wavenumber transform spectra. This work provides an optimum design procedure with the application of GA to successfully determine the optimal location of PZT actuator for sound radiation control of a simply-supported beam. The sensor and actuator design enhances the application of intelligent material structure system to the active structural acoustic control.

ACKNOWLEDGMENTS

The author gratefully acknowledges the support of the work by National Science Council, Republic of China, under grant NSC85-2212-E-020-001.

REFERENCE

[1] C.A. Rogers, "Intelligent Material Systems-The Dawn of a New Materials Age" *Journal of Intelligent Material Systems and Structures*, **4**, 4-12 (1993)

[2] C.A. Rogers, "An Introduction to Intelligent Material Systems and Structures" *Smart Materials, Structures and Mathematical Issues*, 3-41 (1989)
[3] B.T. Wang, "The Performance of Accelerameters and PVDF Sensors in Active Structural Vibration Control" *Bulletine of National Pingtung Polytechnic Institute*, **3**, 81-92 (1994)
[4] B.T. Wang, "The Performance of Accelerometers, Microphones and PVDF Sensors in Active Structural Acoustic Control: Theoretical Analysis" *The Chinese Journal of Mechanics*, **10**, 191-199 (1994)
[5] B.T. Wang, "Active Control of Far-Field Sound Radiation by a Beam with Piezoelectric Control Transducers: Physical System Analysis" *Smart Materials Structures*, **3**, 476-484 (1994)
[6] R.L. Clark and C.R. Fuller, "Control of Sound Radiation with Adaptive Structures" *Journal of Intelligent Material Systems and Structures*, **2**, 431-452 (1991)
[7] R.L. Clark and C.R. Fuller, "Active Structural Acoustic Control with Adaptive Structures Including Wavenumber Considerations" *Journal of Intelligent Material Systems and Structures*, **2**, 431-452 (1992)
[8] R.L. Clark, R.A. Burdisso, and C.R. Fuller, "Design Approaches for Shaping Polyvinylidene Fluoride Sensors in Active Structural Acoustic Control (ASAC)" *Journal of Intelligent Material Systems and Structures*, **4**, 354-365 (1993)
[9] L. Meirovitch and S. Thangjitham, "Control of Sound Radiation Pressure" *Journal of Vibration and Acoustics*, **112**, 237-244 (1990)
[10] C.R. Fuller and J.D. Jones, "Influence of Sensor and Actuator Location on the Performance of Active Control Systems" *presented at the ASME Winter Annual Meeting, 87-WA/NCA-9*, (1987)
[11] T. Bailey and J.E. Hubbard, "Distributed Piezoelectric-Polymer Active Vibration Control of a Cantilevered Beam" *Journal of Guidance Control*, **6**, 605-611 (1986)
[12] R.L. Clark and C.R. Fuller, "Modal Sensing of Efficient Acoustic Radiators with PVDF Distributed Sensors in Active Structural Acoustic Approaches" *Journal of Acoustical Society of America*, **91**, 3321-3329 (1992)
[13] C.K. Lee and F.C. Moon, "Modal Sensors/Actuators" *Journal of Applied Mechanics*, **57**, 434-441 (1990)
[14] F. Fahy, Sound and Structural Vibration (Academic, Orlando, Florida, 1985)
[15] C.R. Fuller and R.A. Burdisso, "A Wavenumber Domain Approach to the Active Control of Structure-borne Sound" *Journal of Sound and Vibration*, **148**, 355-360 (1991)
[16] J.P. Maillard and C.R. Fuller, "Advanced Time Domain Wave-Number Sensing for Structural Acoustic Systems: I. Theory and Design" *Journal of Acoustical Society of America*, **95**, 3252-3261 (1994)
[17] J.P. Maillard and C.R. Fuller, "Advanced Time Domain Wave-Number Sensing for Structural Acoustic Systems: II. Active Radiation Control of a Simply Supported Beam" *Journal of Acoustical Society of America*, **95**, 3262-3272 (1994)
[18] B.T. Wang, "The Development of PVDF Based Wavenumber Domain Model Reference Sensing Technique" *NSC Report*, **NSC84-2212-E-020-005**, (1995)
[19] J.E. Hubbard, "Distributed Sensors and Actuators for Vibration Control in Elastic Components" *Noise-Con 87*, 407-412 (1987)
[20] L. Cremer, M. Heckl, and C.A. Ungar, Structure-Borne Sound (Springer, Berlin, 1973)
[21] H.C. Lester and C.R. Fuller, "Active Control of Propeller Induced Noise Fields Inside a Flexible Cylinder" *AIAA Journal*, **28**, 1374-1380 (1990)
[22] B.T. Wang, "Dynamic Simulation of Hybrid Active and Passive Control of Structural Vibration" *NSC Report*, **NSC81-0401-E-020-501**, (1992)
[23] D.E. Goldberg, Genetic Algorithms in Search, Optimization and Machine Learning (Addison-Wesley, 1989)
[24] B.T. Wang, "Application of Genetic Algorithms to the Optimum Design of Active Control Systems" *Proceedings of International Noise and Vibration Control Conference*, 231-236 (1993)
[25] Inc. Piezo Systems, Product Catalog (1990)
[26] Pennwalt Corporation, Piezo Film Sensor Application Notes (1990)
[27] J. Jia, "Optimization of Piezoelectric Actuator Design in Vibration Control Systems" *Ph.D.Thesis, Department of Mechanical Engineering, Virgina Polytechnic Institute and State University*, (1990)
[28] E.K. Dimitriadis, C.R. Fuller, and C.A. Rogers, "Piezoelectric Actuators for Distributed Vibration Excitation of Thin Plate" *Journal of Vibration and Acoustics*, **113**, 100-107 (1991)
[29] B.T. Wang, R.A. Burdisso, and C.R. Fuller, "Optimal Placement of Piezoelectric Actuators for Active

Structural Acoustic Control" *Journal of Intelligent Material Systems and Structures*, **5**, 67-77 (1994)
[30] C.E. Wallace, "Radiation Resistance of a Rectangular Panel" *Journal of Acoustical Society of America*, **51**, 946-952 (1972)
[31] C.E. Wallace, "Radiation Resistance of a Baffled Beam" *Journal of Acoustical Society of America*, **51**, 936-945 (1972)
[32] H. Peng, and P. Banks-Lee, "Edge Effect on Radiation Efficiency of a Baffled Beam Below the Critical Frequency" *Journal of Acoustical Society of America*, **88**, 2001-2006 (1990)

Table 1. Optimal location of PZT actuators for the CWT approach

excitation frequency (Hz)	$\Phi_{\tilde{A}}$ x1,x2	$\Phi_{\tilde{V}}$ x1,x2
33.2	0.128581,0.192081	0.067538,0.131038
100	0.121264,0.184764	0.090018,0.153518
128.8	0.115600,0.179100	0.116700,0.180200
230	0.084228,0.147728	0.086530,0.150030
290	0.065103,0.128603	0.316130,0.379630

Table 2. Optimal location of PZT actuators for the DWT approach

excitation frequency (Hz)	$\Phi_{\kappa,\tilde{A}_{DWT}}$ x1,x2	$\Phi_{\kappa,\tilde{V}_{DWT}}$ x1,x2
33.2	0.096583,0.160083	0.067026,0.130526
100	0.117434,0.180934	0.127696,0.191196
128.8	0.116700,0.180200	0.116700,0.180200
230	0.084228,0.147728	0.084228,0.147008
290	0.066721,0.130221	0.316130,0.379630

Table 3. Reduction of radiated power (dB)

f (Hz)	$\Phi_{\tilde{A}}$	$\Phi_{\tilde{V}}$	$\Phi_{\kappa,\tilde{A}_{DWT}}$	$\Phi_{\kappa,\tilde{V}_{DWT}}$	Arb.
33.2	96.14	70.14	72.01	62.68	59.69
100	44.25	5.25	33.41	16.15	0.07
128.8	87.22	71.98	81.25	73.08	50.95
230	16.81	11.5	16.58	16.69	0.01
290	76.05	63.25	71.48	60.29	62.57

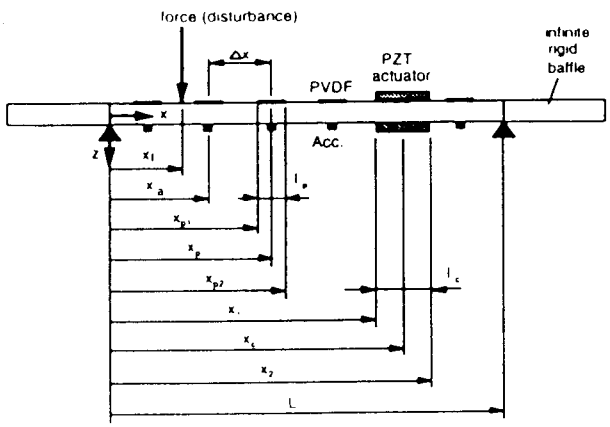

Figure 1. The arrangement and coordinates of simply-supported beam

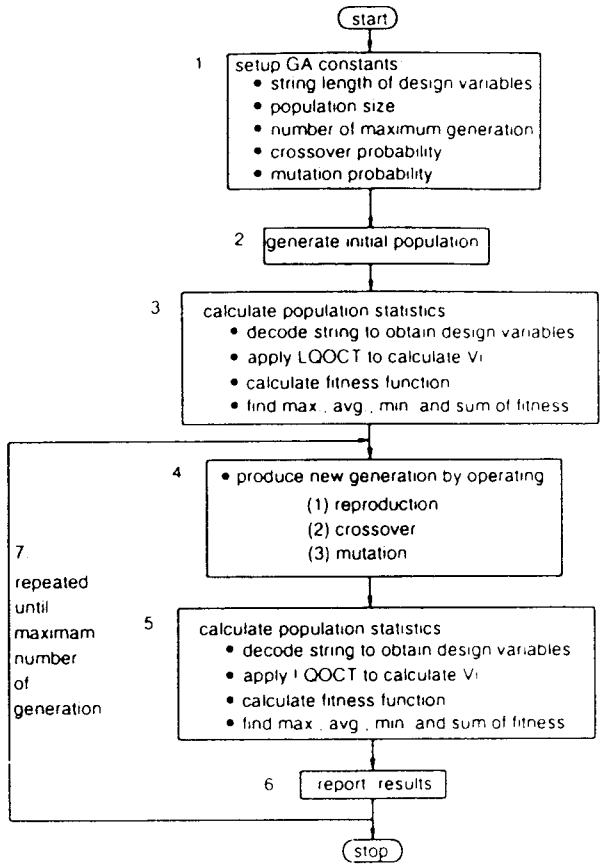

Figure 2. Flow chart of solution procedures

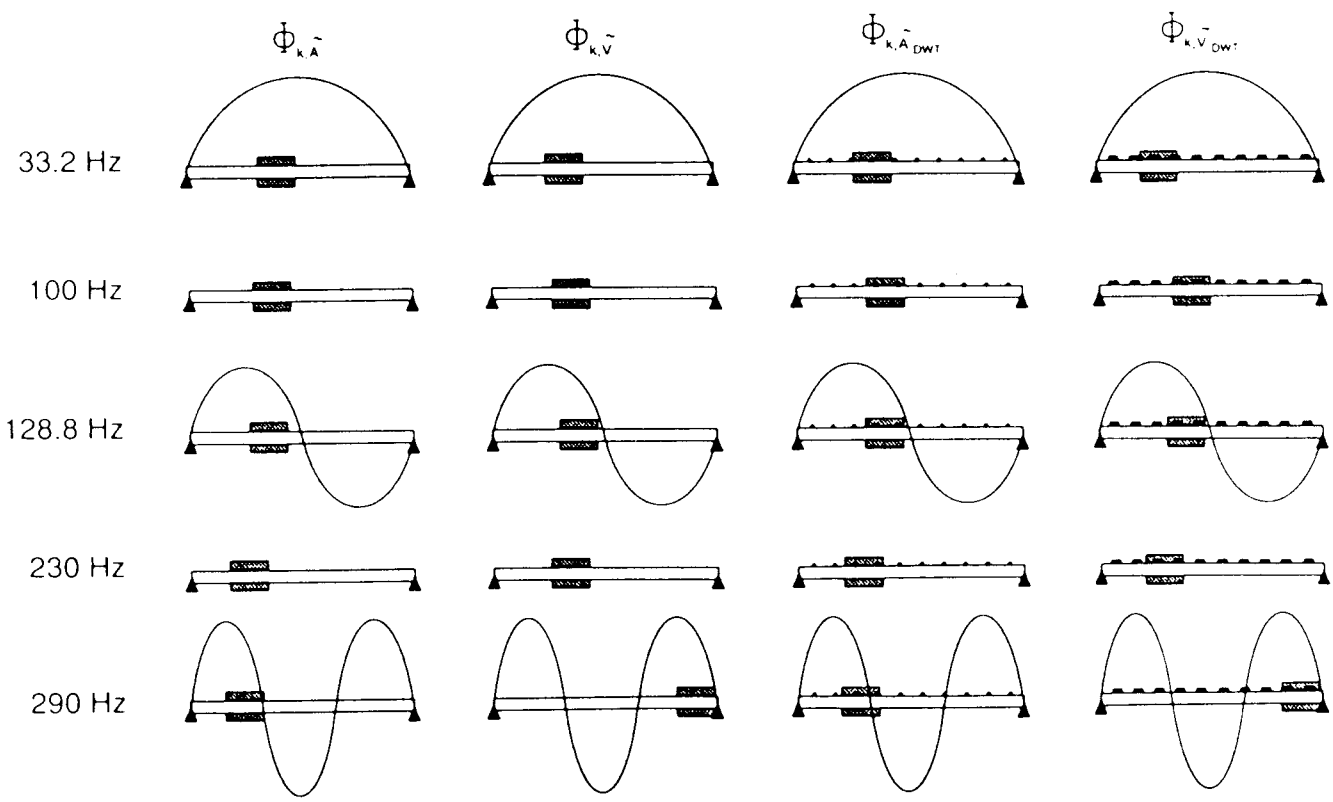

Figure 3. Optimal location of PZT actuators

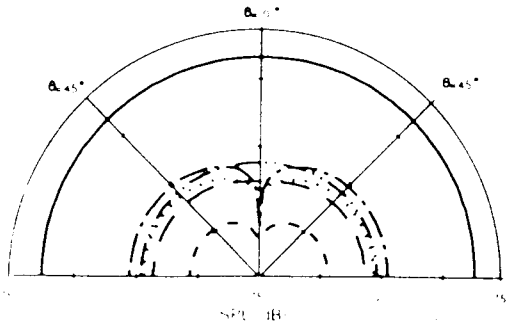

(a) f=33.2Hz

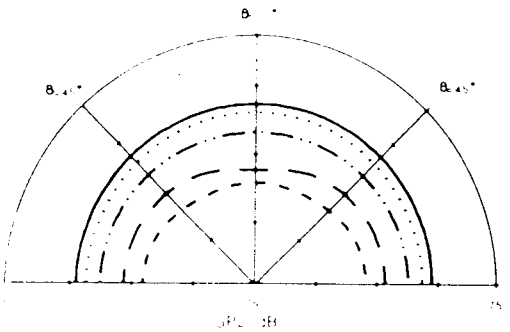

(b) f=100Hz

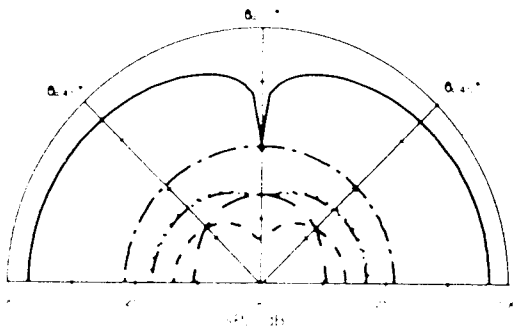

(c) f=128.8Hz

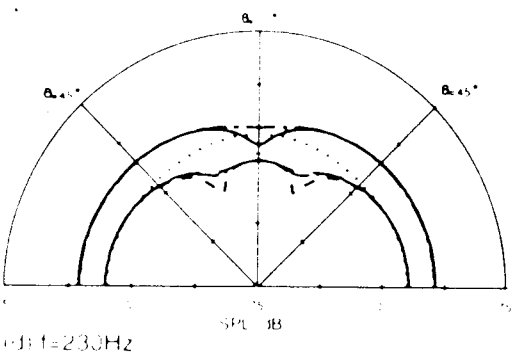

(d) f=230Hz

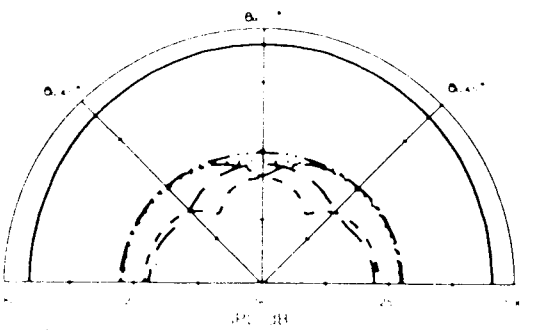

(e) f=290Hz

disturbance $\Phi_{..}$ $\Phi_{..}$ $\Phi_{..}$ $\Phi_{..}$ arb

Figure 4 Sound pressure level distributions

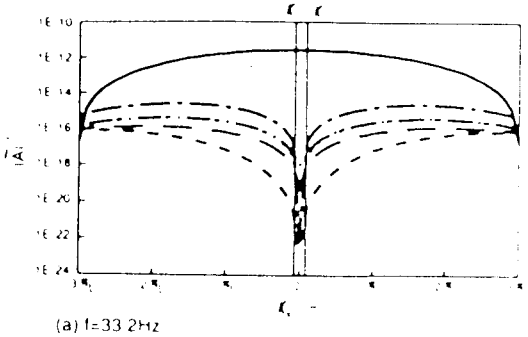

(a) f=33.2Hz

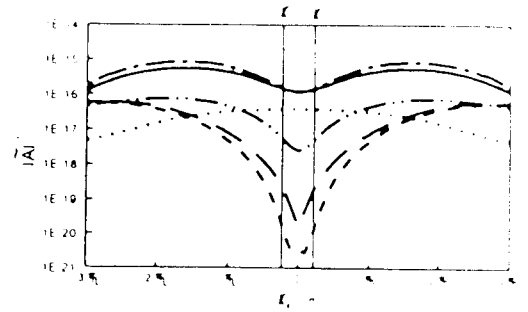

(b) f=100Hz

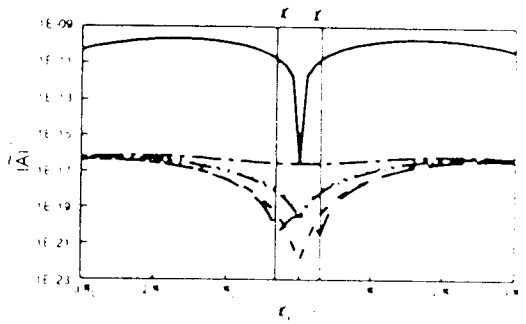

(c) f=128.8Hz

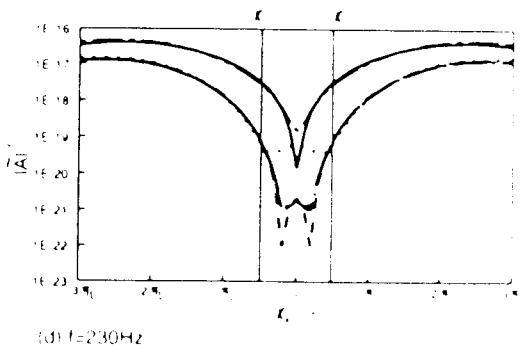

(d) f=230Hz

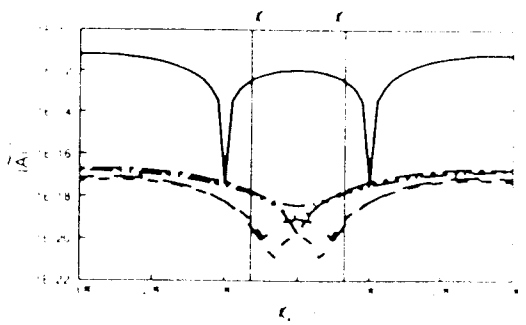

(e) f=290Hz

disturbance $\Phi_{..}$ $\Phi_{..}$ $\Phi_{..}$ $\Phi_{..}$ arb

Figure 5 Acceleration wavenumber spectra